Civil Engineering Dimension
https://ced.petra.ac.id

Performance Analysis of Eccentrically Braced Frames (EBF) using Metallic Yielding Damper (MYD) with Hysteretic Steel Damper (HSD) Type

Suswanto, B.[1]*, Ghifari, F.[2], Triwulan[1], Sugihardjo, H.[1], and Pangestuti, P.A.[1]
[1] Department of Civil Engineering, Institut Teknologi Sepuluh Nopember (ITS), Surabaya 60111, INDONESIA
[2] Ph.D Student of Civil and Construction Engineering, National Taiwan University of Science and Technology (NTUST), Taipei, TAIWAN

DOI: https://doi.org/10.9744/ced.27.1.1-11

Article Info:
Submitted: Jul 20, 2024
Reviewed: Aug 12, 2024
Accepted: Feb 13, 2025

Keywords:
eccentrically braced frames,
vertical link,
metallic yielding damper,
hysteresis steel damper,
shear capacity,
dissipated energy.

Corresponding Author:
Suswanto, B.
Department of Civil Engineering,
Institut Teknologi Sepuluh Nopember
(ITS), Surabaya 60111, INDONESIA
Email: budi_suswanto@its.ac.id

Abstract

Eccentrically Braced Frames (EBFs) are earthquake-resistant steel structures with excellent shear capacity and ductility. During earthquakes, the EBF link yields first, protecting other structural elements. Traditionally, the link is integrated with the main beam and separated by bracing. However, if the link is damaged, replacing the entire beam becomes necessary. To address this, a vertical link design allows for link replacement without altering the beam section. This study evaluates two vertical link options: a Wide Flange (WF) link section and a Hysteretic Steel Damper (HSD) type Metallic Yielding Damper. Results suggest the WF link is preferable due to superior shear capacity and energy dissipation compared to the HSD link. The findings recommend the WF link for vertical link EBFs to optimize earthquake performance.

INTRODUCTION

Steel structure construction is one of the earthquake-resistant structural systems with good performance. In general, the purpose of creating an earthquake-resistant structural system design is to avoid partial collapse mechanisms and soft-story collapse mechanisms that can significantly damage the energy dissipation capacity of the structure [1]. With the properties of steel materials that are ductile, high strength, and good energy dissipation ability, the steel structure is very suitable when used in areas with a high seismic activity. One of the earthquake-resistant steel structure systems based on Bruneau et al. [2] is Eccentrically Braced Frames (EBF), which prioritizes the strength and stiffness of the vertical frame system as a support for lateral loads and has bracing elements as stiffeners and strengthens the structure. Eccentrically braced frames (EBF) are the structural system that limits inelastic behavior only to the link beam that is between two eccentric restraints, while the outer beams, columns, and diagonal restraints remain elastic during seismic loads [3]. Meanwhile, according to Mansour et al. [4], eccentrically braced frame (EBF) is a lateral seismic load-bearing system that includes ductility and energy dissipation in beam elements called links. The design of eccentrically braced frames (EBF) depends on the strength, stiffness, and ductility of the system, which is related to link dimensions, link length, and details. The main function of the link is a pre-melted element of all Eccentrically Braced Frames (EBF) components, which have a plastic deformation capacity and can dissipate the energy released by an earthquake [5]. Link must be designed as the weakest part of a structural member with behavior as a system "fuse" in a structural system [6]. Other Eccentrically Braced Frame (EBF) components, such as beams, columns, and bracings remain elastic. The moments generated at both ends of the link have the same magnitude and direction due to the shear force acting on both ends of the beam [7]. The length of the link is denoted by "*e*", as shown in Figure 1.

Note : Discussion is expected before July, 1st 2025, and will be published in the "Civil Engineering Dimension", volume 27, number 2, September 2025.
ISSN : 1410-9530 print / 1979-570X online
Published by : **Petra Christian University**

In general, eccentrically braced frames (EBF) have two types of links, there are EBF with horizontal links (H-EBF) and EBF with vertical links (V-EBF), as shown in Figure 1(a) and Figure 1(b), respectively. Eccentrically braced frames with horizontal links (H-EBF) can dissipate energy well, but when an earthquake occurs which causes inelastic rotation, the link will rotate vertically [8]. In the H-EBF link, the links are merged with the beam so that repairing or replacing a damaged link on the H-EBF after a major earthquake can be very difficult and disrupt other structural systems [4]. Additionally, a repeated inelastic deformation can cause a local buckling on the whole beam after a large earthquake event [9]. Therefore, the solution is to use V-EBF where it is possible to repair or replace damaged link elements after a large earthquake, without replacing or changing parts of the beam [10]. Research by Shayanfar et al. [11] shows that Eccentrically Braced Frames with vertical links (V-EBF) have advantages over the H-EBF system, including ductility, high elastic strength, functionality as a ductile fuse system, and effectiveness in the disassembly process after damage occurs, without disturbing other structural elements. Meanwhile, based on Bouwkamp et al. [12], in the V-EBF system inelastic deformation occurs throughout the link, so there is no damage to the main components such as beams and columns, and structural repairs after a strong earthquake are easier than H-EBF. According to Daneshmand and Hashemi [13], the length of the link is divided into 3 types, namely short links (sliding links), intermediate links (immediate links), and long links (flexible links). Short links or sliding links are recommended in terms of strength capacity, ductility, and stiffness [14].

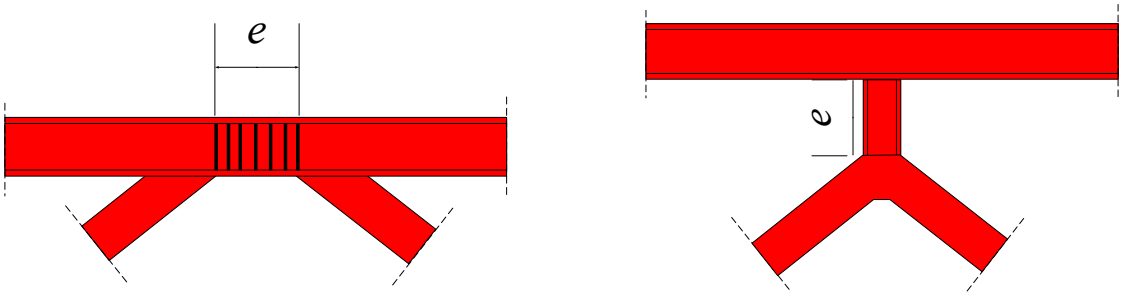

(a) Horizontal Link (b) Vertical Link

Figure 1. The Definition and Types of Links

The structure will experience a decrease in capacity and even structural failure due to seismic events. Therefore, the structure requires a reparation which can be retrofitting or replacing the installation of new materials (replaceable). The procedure for retrofitting or replacing the existing structural must conform to the code and the existing conditions of the structure. Adding or replacing new seismic retaining elements in the structure with the aim of increasing its capacity must pay attention to parameters such as strength reduction factor, force to weight ratio, ductility, period, etc. [15]. The experimental design of some types of metallic yielding damper (MYD) has been tested by Aghlara et al. [16] with specimens tested, including: Triangular-plate Added Damping and Stiffness, Cast Steel Yielding Brace, Dual-Pipe Damper, Infilled-Pipe Damper, Yielding Shear Panel Device, Hysteretic Steel Damper, and Dual Function Metallic Damper. The results of the study [16] state the classification of the type of failure on each damper. The failure of shear on section occurred in the dual-pipe damper type, infilled-pipe damper type, and yielding shear panel device type. The failure of the bending of the plate occurred in the Cast Steel Yielding Brace type and the Triangular Plate Added Damping and Stiffness type. The failure of shear in the plate occurred in the hysteresis steel damper type and dual function metallic damper type. Structures with additional dampers are often used to meet occupant safety and comfort requirements during earthquakes and increase the economic efficiency of building use [17]. Based on Benavent-Climent [18], the use of dampers can reduce the damage to structural and non-structural elements. The reparation after the earthquake event can be carried out with minimal costs and do not interfere with other structural elements.

METHOD

This study will analyze the EBF system using vertical links, where the links are installed vertically, connecting the beams and bracings. Some analyses are carried out with various types of link sections: wide flange (WF) section links and metallic yielding damper (MYD) links, which are dampers in the form of pure steel plates with the purpose of getting better results in terms of ductility, shear capacity, and energy dissipation. The MYD links used is the Hysteretic Steel Damper (HSD) type, which has previously been experimentally carried out by Teruna et al. [19]. Mild steel plates with different geometrical shapes are used to evaluate the energy absorption of the HSD, as shown in Figure 2. Four types of V-EBF were prepared by Teruna et al. [19] including type 1 HSD link (V-EBF-HSD1), type 2 HSD link (V-EBF-HSD2), type 3 HSD link (V-EBF-HSD3), and type 4 HSD link (V-EBF-HSD4). In this study, a modified HSD link based on Teruna et al. [19] is proposed to compare and evaluate the seismic capacity of

the Links. The proposed HSD links are shown in Figure 3. Every proposed HSD section has a difference in the value of the center curvature that affects the dimensions and performance values of the HSD.

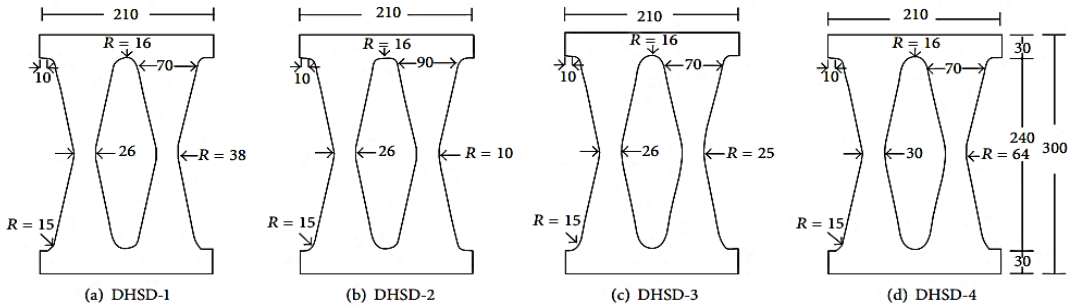

Figure 2. The Dimension of HSD bsed on Teruna Et al. [19] (Unit: mm)

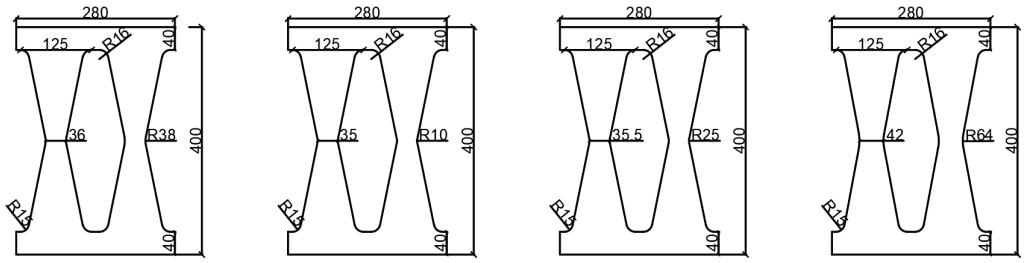

Figure 3. The Dimension of the Proposed HSD (Unit: mm)

Materials

In this study, two different steel grades are used. To convince that the failure is at the Link, the strength of Links is intentionally designed to be lower than the beam, columns, and braces. Therefore, ASTM-A36 is used for Links with the yield strength of 292 MPa, whereas the beam, columns, and braces use ASTM-A992 with the yield strength of 345 MPa. The detail information of the material is tabulated in Table 1. Additionally, the stress-strains used are shown in Figure 4 and Figure 5.

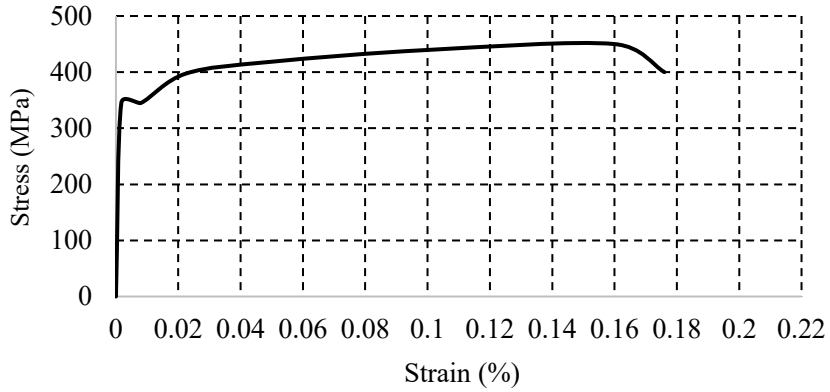

Figure 4. ASTM-A992 Stress-strain Curve

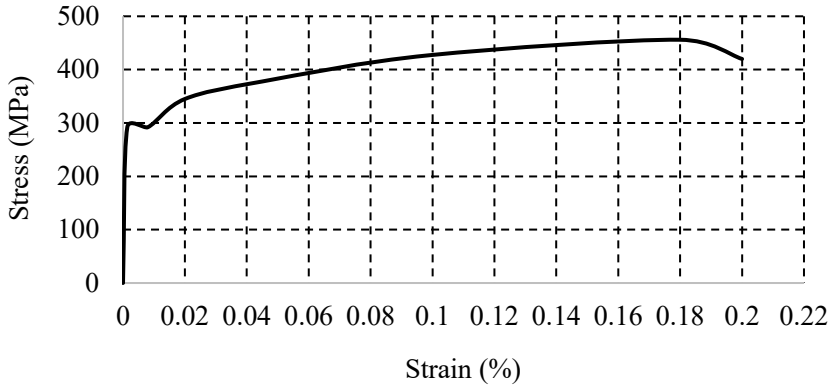

Figure 5. ASTM-A36 Stress-strain Curve

Table 1. Material Definition

ASTM-A992		ASTM-A36	
f_y (MPa)	345	f_y (MPa)	292
f_u (MPa)	450	f_u (MPa)	456
Density (kg/m^3)	7850	Density (kg/m^3)	7850
E_s (MPa)	200000	E_s (MPa)	210000
Poisson's ratio	0.3	Poisson's ratio	0.3
e_{max} (%)	18%	e_{max} (%)	16

Notes: f_y and f_u are the yield and ultimate strength, respectively; E_s is the Young's modulus of steel; e_{max} is the maximum strain of steel

Modeling and Loading Protocol

In this study, ABAQUS CAE software is used to perform a Finite Element (FE) analysis. Before the FE analysis is performed, the steel section used is in accordance with the preliminary design that has been determined and has been analyzed using SAP2000 software according to the existing structural conditions. Based on Moestopo et al. [20], the procedures to design a structure are determining the dimensions or geometries, connection design, designing the elements outside the links with capacity design concepts, and checking the failure mechanisms. Based on preliminary design results, the steel section used is tabulated in Table 2.

Table 2. The Steel Section Dimension Used

No.	Model	Column	Beam	Link	Bracing
1	V-EBF-WF	KC800x300x14x26	WF600x200x11x17	WF500x200x10x16	WF600x200x11x17
2	V-EBF-HSD1			HSD type 1	
3	V-EBF-HSD2			HSD type 2	
4	V-EBF-HSD3			HSD type 3	
5	V-EBF-HSD4			HSD type 4	

The modeling of the V-EBF frame specimen at Abaqus CAE starts with the geometry modeling stage (module part). This stage constructs the shape of each element on the frame based on the dimensions that have been determined. The model setup is shown in Figure 6 and Figure 7. The depiction of parts in the form of 3-dimensional solid elements in Abaqus CAE can be done by directly drawing each coordinate from the cross section, or it can be done by importing images from AutoCAD software, then uniting the parts that have been made in the form of frames with the Assembly module. Then input the material properties as listed in Table 1. Parts that have been assembled are installed with a tie-constraint type of surface-to-surface interaction. The next stage is the provision of boundary conditions (BC) to define the location of the support and the location of the cyclic loading. The support frame is at the bottom end of the column or column foot and is given the type of fixed or clamped support. The top end of the column is given a boundary condition (BC) for cyclic loading.

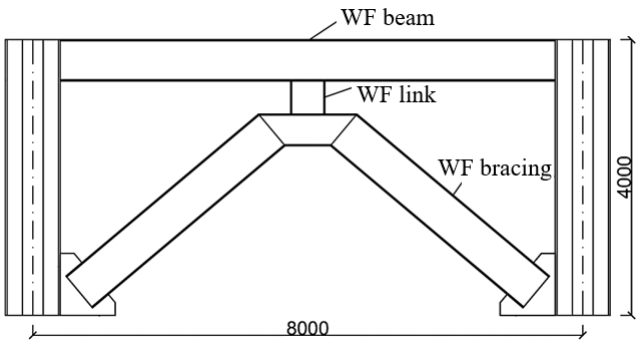

Figure 6. The Modeling of V-EBF-WF Type (Unit: mm)

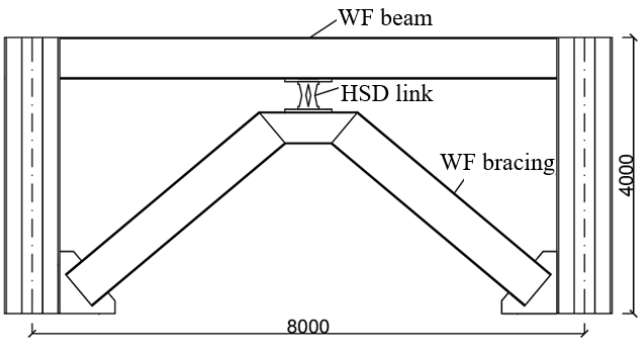

Figure 7. The Modeling of V-EBF-WF Type (Unit: mm)

The loading protocol is based on AISC 341 [21]. The loading is given in stages and begins with a static push load of 0.00375 rad. The total cyclic load applied during the analysis is 32 cycles, consisting of 32 pushes and 32 pulls. Detailed details of the loading protocol values can be seen in Figure 8 and Table 3. The next stage in the frame modeling process is meshing. The meshing types used are C3D8R for beams, columns, and bracing, and C3D6 types for links. The evaluations of the V-EBF modeling analysis are frame shear capacity, hysteresis curve, energy dissipation, link failure pattern, and structural ductility. Furthermore, the performance of each specimen of the V-

EBF frame is compared to obtain the results of the V-EBF frame with the recommended link type based on the evaluation parameters.

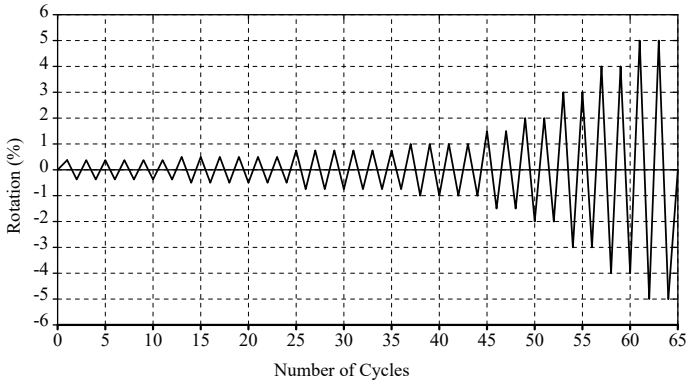

Figure 8. The Loading Protocol based on AISC 341-16

Table 3. The Magnitude of the Loading Protocol based on AISC 341-16

No.	Rotation (rad)	Displacement (mm)	Cyclic Number
1	0.00375	15	6
2	0.005	20	6
3	0.0075	30	6
4	0.01	40	4
5	0.015	60	2
6	0.02	80	2
7	0.03	120	2
8	0.04	160	2
9	0.05	200	2
Total cycle			32

RESULTS AND DISCUSSION

V-EBF-WF Model

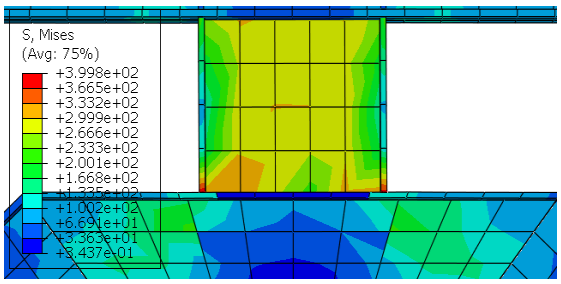

(a) WF Link Failure at Yield Stress Level (MPa)

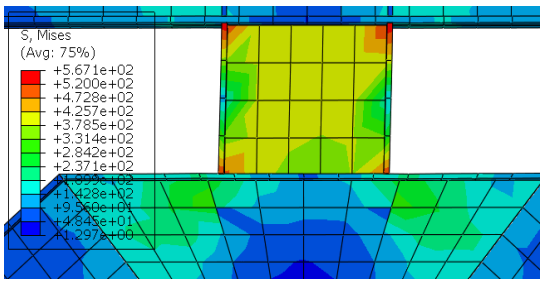

(b) WF Link Failure at Ultimate Stress Level (MPa)

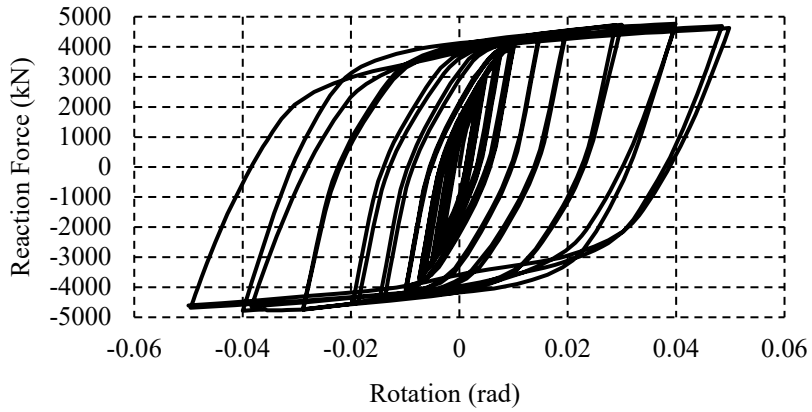

(c) Hysteresis Curve of V-EBF-WF Model

Figure 9. The Numerical Results of V-EBF-WF Model

Figure 9 presents the numerical results of V-EBF-WF model. The failure condition of the WF link when it reaches the yield stress value (f_y) is shown in Figure 9(a). The WF link experiences yielding that occurs in the same area, namely at the web link and the flange link end, and the highest stress is at the flange link end. The first yield occurred at a drift ratio of 0.13% rad with the yield force of 1266.57 kN. Furthermore, the WF link reaches its ultimate value in the same area when yielding occurs, as shown in Figure 9(b). The hysteresis curve in the analysis of the V-EBF-WF specimen shows that the peak force absorbed by the specimen is 4,782.61 kN under displacement conditions of 159.805 mm, or equivalent to a rotation of 0.0399 rad, as shown in Figure 9(c). Eccentrically Braced Frame (EBF) with this WF link can dissipate an energy of 2,328,243 kNm. So, from the analysis results, the ductility of the V-EBF-WF frame specimen is 30.427.

V-EBF-HSD1 Model

The numerical results of V-EBF-HSD1 model are presented in Figure 10. Figure 10(a) shows the failure condition of the HSD1 link. When it reaches the yield stress value (f_y), the HSD1 link begins to experience yielding that occurs in the HSD1 plate body in the inner curvature (R16) and outer curvature (R15) of the top and bottom to the length and almost the width of the plate edge body before the center bend (R38). The link experienced a first yielding at a drift ratio of 0.131% with the yield force of 693.06 kN. Furthermore, the HSD1 link begins to reach the initial ultimate condition in the HSD1 plate body in the upper and lower inner bend (R16) and outer bend (R15) edges of the plate along the plate edge before the middle bend (R38), as during the initial yielding, for the plate inner area. Until the bend area R38 has reached the yield stress value almost evenly throughout the slab area, except for the end area of the connection to the floor beams and gusset slabs, as shown in Figure 10(b). The hysteresis curve on the analysis results of the V-EBF-HSD1 model is shown in Figure 10(c). The peak force absorbed by the specimen is 3955.21 kN at a displacement of 199.411 mm or equivalent to a rotation of 0.0498 rad. EBF with type 1 HSD link can dissipate an energy of 2018, 202 kN.m. So, from the results of the analysis, the ductility of the V-EBF-WF frame specimen is 37.961.

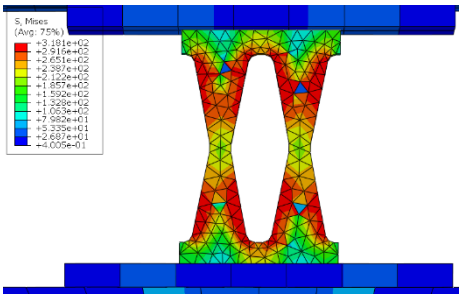

(a) HSD1 Link Failure at Yield Stress Level (MPa)

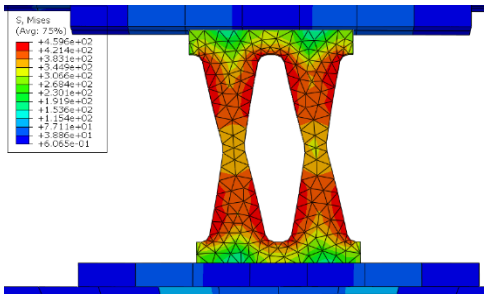

b) HSD1 Link Failure at Ultimate Stress Level (MPa)

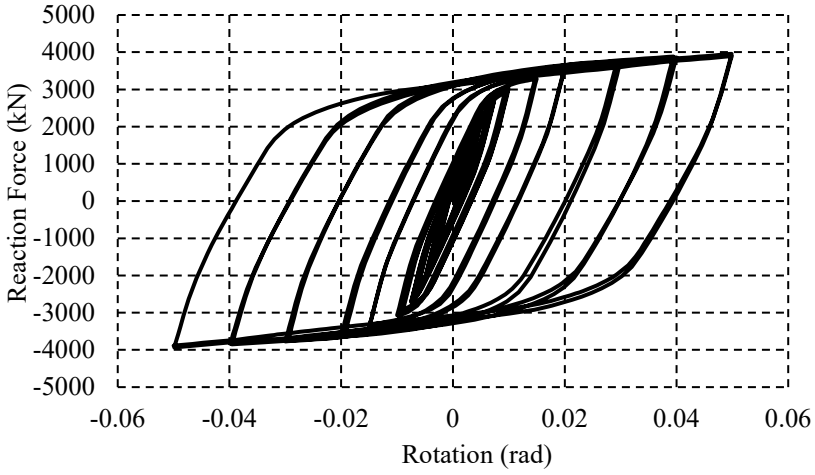

(c) Hysteresis Curve of HSD1 Model

Figure 10. The Numerical Results of V-EBF-HSD1 Model

V-EBF-HSD2 Model

Figure 11 represent the result of the V-EBF-HSD2 model. When it reaches the yield stress value (f_y), the HSD2 link begins to experience yielding at a drift ratio of 0.131% and occurs in the HSD2 plate body in the inner bend (R16)

and outer bend (R15) top and bottom to the length and almost the width of the plate edge body before the center bend (R10), as shown in Figure 11(a). The yield strength produced by HSD2 model is 692.8 kN. Furthermore, the HSD2 link begins to reach the initial ultimate condition in the HSD2 plate body in the upper and lower inner curvature (R16) and outer curvature (R15) along the plate edge up to before the middle curvature (R10), as during the initial yielding, for the plate inner area. Until the bend area R10 has reached the yield stress value almost evenly throughout the slab area except for the end area of the connection to the floor beams and gusset slabs as shown in Figure 11(b). The hysteresis curve of the V-EBF-HSD2 is shown in Figure 11(c). The model shows that the peak force absorbed by the model is 3945.93 kN at a displacement of 199.791 mm or equivalent to a rotation of 0.0499 rad as shown in Figure 11(c). EBF with HSD type 2 link can dissipate an energy of 2014.499 kN-m. So, from the analysis results the ductility of the V-EBF-WF frame specimen is 38.034.

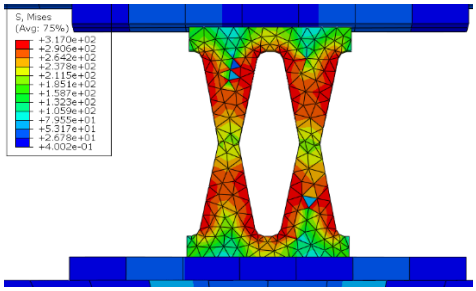

(a) HSD2 Link Failure at Yield Stress Level (MPa)

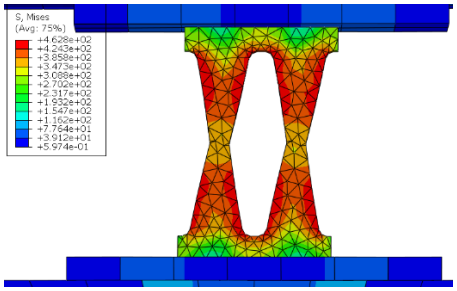

(b) HSD2 Link Failure at Ultimate Stress Level (MPa)

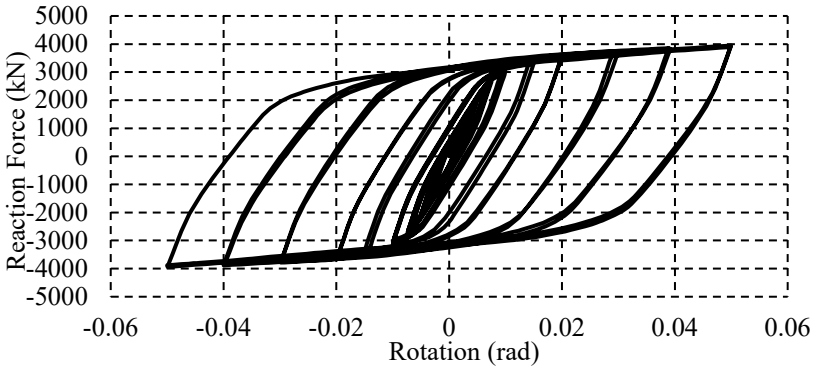

(c) Hysteresis Curve of HSD2 Model

Figure 11. The Numerical Results of V-EBF-HSD2 Model

V-EBF-HSD3 Model

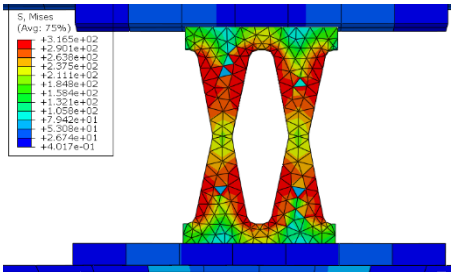

(a) HSD3 Link Failure at Yield Stress Level (MPa)

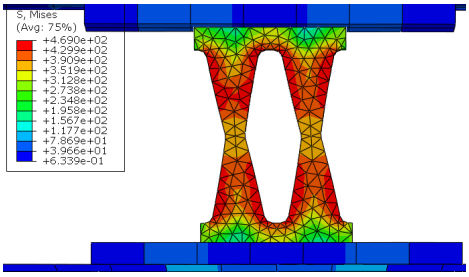

(b) HSD3 Link Failure at Ultimate Stress Level (MPa)

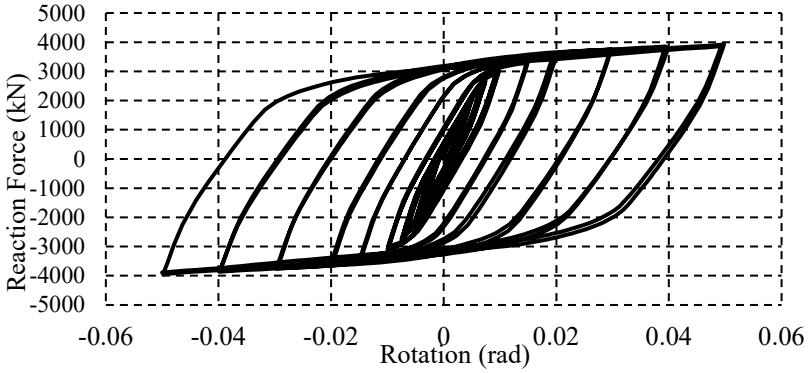

(c) Hysteresis Curve of HSD3 Model

Figure 12. The Numerical Results of V-EBF-HSD3 Model

Figure 12 shows the results of the V-EBF-HSD3 model. The failure condition of the HSD3 link when it reaches the yield stress value (f_y), the HSD3 link begins to experience yielding at a drift ratio of 0.131% that occurs in the HSD3 plate body in the inner bend (R16) and outer bend (R15) of the top and bottom to the length and almost the width plate edge body before the center bend (R25), as shown in Figure 12(a). Additionally, the yield strength of HSD3 is 693.56 kN. Furthermore, the HSD3 link begins to reach the initial ultimate condition in the HSD3 plate body in the upper and lower inner bend (R16) and outer bend (R15) edges of the plate along the plate edge to before the middle bend (R25) as at the beginning of yielding, for the plate inner area. until the bend area R25 has reached the yield stress value almost evenly throughout the slab area except for the end area of the connection to the floor beams and gusset slabs as shown in Figure 12(b). The hysteresis curve on the analysis results of the V-EBF-HSD3 model shows that the peak force absorbed by the specimen is 3951.96 kN at a displacement of 199.224 mm or equivalent to a rotation of 0.0498 rad as shown in Figure 12(c). EBF with type 3 HSD link can dissipate an energy of 2015.449 kNm. So, from the results of the analysis, the ductility of the V-EBF-WF frame specimen is 37.926.

V-EBF-HSD4 Model

Figure 13(a) shows the failure condition of the HSD4 link. When it reaches the yield stress value (f_y), the HSD4 link begins to experience yielding at a drift ratio of 0.131% that occurs in the HSD4 plate body in the area of the inner bend (R16) and outer bend (R15) top and bottom to the length and almost the width plate edge body before the center bend (R64). HSD4 produces a yield strength of 701.128 kN. Furthermore, the HSD4 link begins to reach the initial ultimate condition in the HSD4 plate body in the upper and lower inner bend (R16) and outer bend (R15) edges of the plate along the plate edge until before the middle bend (R64) as during the initial yielding, for the plate inner area. Until the bend area R64 has reached the yield stress value almost evenly throughout the slab area except for the end area of the connection to the floor beams and gusset slabs as shown in Figure 13(b). The hysteresis curve in the analysis of the V-EBF-HSD4 specimen shows that the peak force absorbed by the model is 4022.15 kN at a displacement of 199.928 mm or equivalent to a rotation of 0.0499 rad as shown in Figure 13(c). Eccentrically Braced Frame (EBF) with type 4 HSD link can dissipate an energy of 2026.373 kNm. So, from the results of the analysis, the ductility of the V-EBF-WF frame specimen is 38,060.

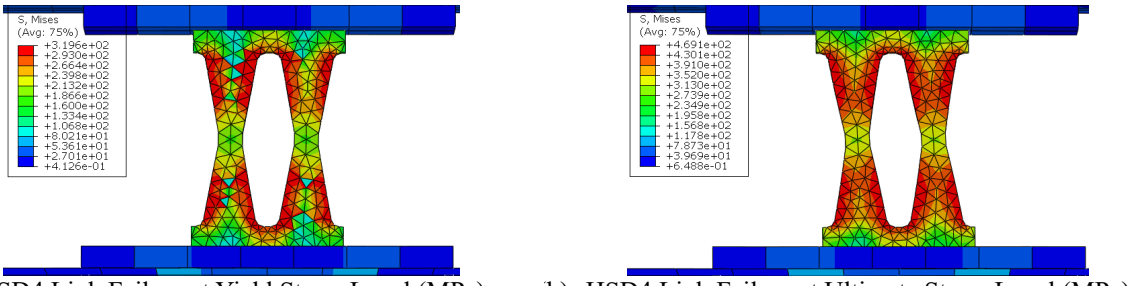

(a) HSD4 Link Failure at Yield Stress Level (MPa) b) HSD4 Link Failure at Ultimate Stress Level (MPa)

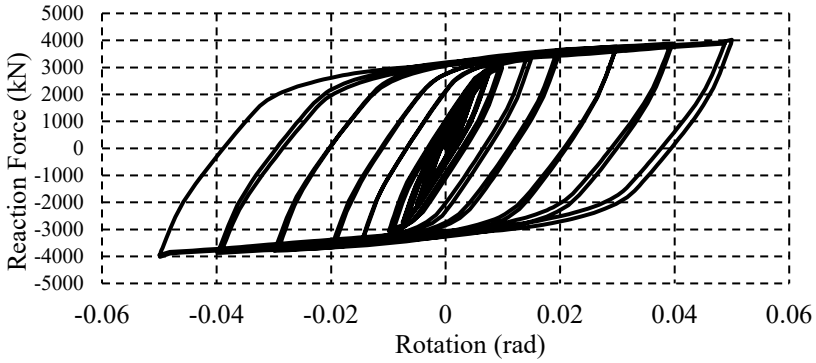

(c) Hysteresis Curve of HSD4 Model

Figure 13. The Numerical Results of V-EBF-HSD4 Model

Seismic Performance Comparison of EBF System between WF and HSD Link

To evaluate the seismic performance of each system, a comparison in terms of energy dissipation and ductility is observed. Energy dissipation is the ability of a structural member to absorb energy under an earthquake, which can be defined by the equivalent viscous damping coefficient ζ_{eq} and cumulative energy dissipation area (E_{sum}) [22], as described in Figure 14. ζ_{eq} and E_{sum} can be calculated as:

$$\zeta_{eq\_i} = \frac{1}{2\pi}\left(\frac{E_{loop\_i}}{E_{e+\_i} + E_{e-\_i}E_{loop\_i}}\right) \quad (1)$$

$$E_{sum} = \sum_{i=1}^{n} E_{loop\_i} \quad (2)$$

where E_{e+_i}, and E_{e-_i} are the elastic strain energy for each i cycle, E_{loop_i} is the energy dissipation for each i cycle, and n is the cycle number. The energy dissipation is calculated based on the peak strength for each cycle. The energy dissipation in each specimen is directly proportional to the reaction force value, the greater the reaction force value, the greater the energy dissipation value, as listed in Table 5.

On the other hand, ductility is the capability of the member or system to deform in an excessive deformation without any failure [23]. In general, ductility is defined as a ratio between the ultimate and the first yield deformation, which is obtained from the backbone curve as shown in Figure 15. The result of the ductility index is tabulated in Table 6.

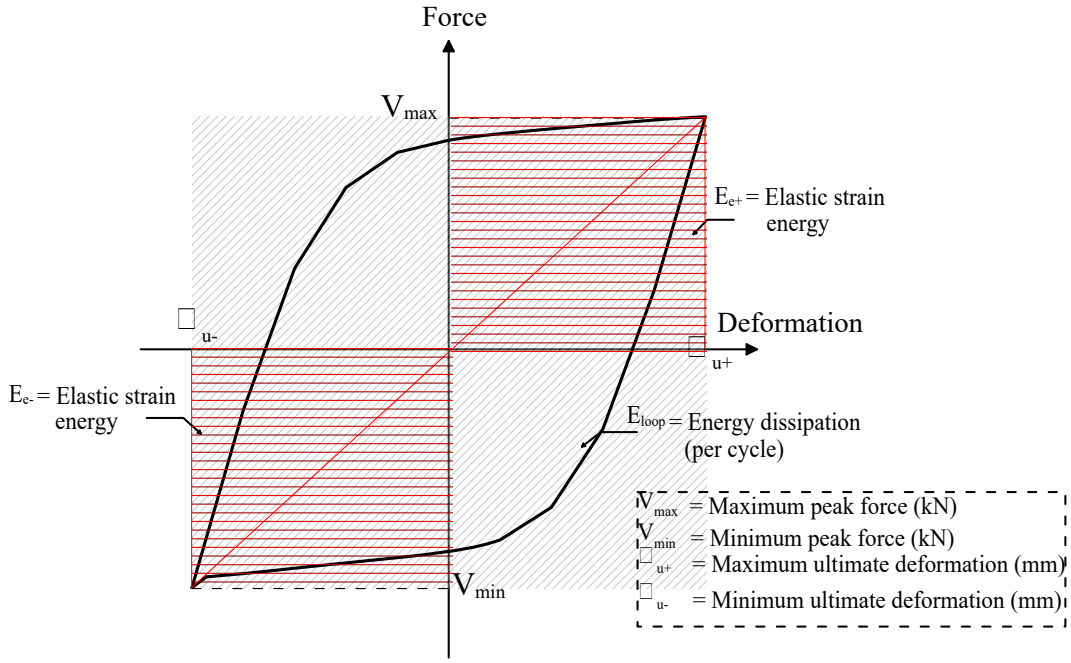

Figure 14. Definition of the Equivalent Viscous Damping Equation

Table 4. Comparison of the Reaction Force of All Models

No	Model	Peak reaction force (kN)	Difference with the WF link (%)
1	V-EBF-WF	4782.61	-
2	V-EBF-HSD1	3955.21	17.3
3	V-EBF-HSD2	3945.93	17/49
4	V-EBF-HSD3	3951.96	17.37
5	V-EBF-HSD4	4022.15	15.9

Table 5. Comparison of the Energy Dissipation of All Models

No	Model	Energy dissipation (kN-m)	Difference with the WF link (%)
1	V-EBF-WF	2328.24	-
2	V-EBF-HSD1	2018.20	13.32
3	V-EBF-HSD2	2014.49	13.48
4	V-EBF-HSD3	2015.45	13.43
5	V-EBF-HSD4	2026.37	12.96

The backbone curve in Figure 15 shows the difference in performance from the V-EBF-WF modeling with V-EBF-HSD1, V-EBF-HSD2, V-EBF-HSD3, and V-EBF-HSD4, and the reaction forces are tabulated in Table 4. The V-EBF-WF modeling has the largest shear capacity value compared to the V-EBF link HSD specimen. The performance of V-EBF-WF reached the peak value of reaction force in the 29th cycle and then decreased. Unlike the V-EBF link

WF, the modeling of the V-EBF link HSD1, HSD2, HSD3, and HSD4 has a stable performance in increasing the reaction force value, where the peak Reaction Force value occurs in the 31st cycle.

Table 6. Comparison of the Ductility of All Models

No	Model	Δ_y (mm)	Δ_u (mm)	μ	Difference with the WF link (%)
1	V-EBF-WF	5.25	159.8	30.43	-
2	V-EBF-HSD1	5.25	199.41	37.96	19.85
3	V-EBF-HSD2	5.25	199.79	38.03	19.99
4	V-EBF-HSD3	5.25	199.22	37.93	19.77
5	V-EBF-HSD4	5.25	199.93	38.06	20.05

Notes: Δ_y is the Deformation at first yield; Δ_u is the Deformation at ultimate; μ = The ductility index

Comparison of HSD Link Models

Figure 15 shows the backbone curve of four types of hysteresis steel damper (HSD) which shows the performance of each type of HSD obtained from plotting the maximum reaction force value in each loading cycle. HSD1, HSD2, HSD3, and HSD4 links have different radian values in the middle curve, and specifically, HSD4 has different dimension values from other HSD links. The four types of HSD have almost similar performance in the values of reaction force, energy dissipation, and ductility, which are listed in Table 4 to Table 6. The middle curvature of each HSD link affects the value of reaction force, energy dissipation, ductility, and failure pattern on V-EBF performance with HSD links. The results of the analysis using ABAQUS show that the greater the radian value in the middle curvature of the link, the greater the value of the reaction force absorbed, which affects the amount of energy dissipation.

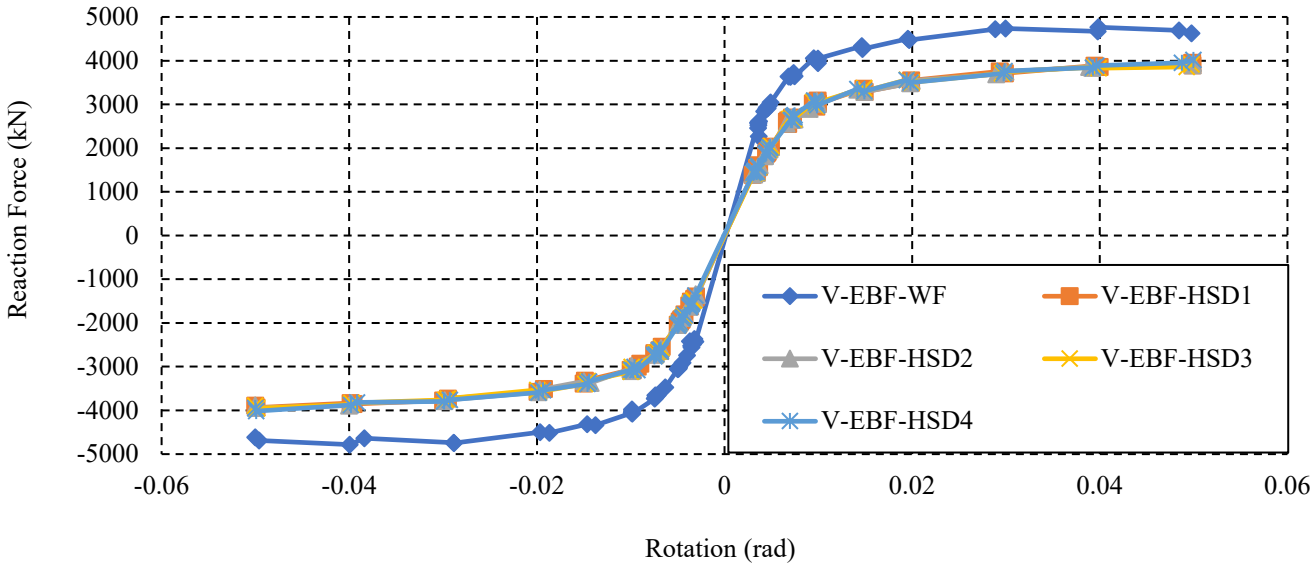

Figure 15. Backbone Curve Comparison

CONCLUSIONS

Based on the research that has been done, the study concludes that EBFs with vertical WF links demonstrate greater shear capacity and energy dissipation compared to HSD links. WF links can absorb 17.3% more shear force than HSD1, 17.49% more than HSD2, 17.37% more than HSD3, and 15.90% more than HSD4. Energy dissipation performance is directly related to shear capacity, with WF links showing an average 13% higher energy dissipation than HSD links. However, HSD links exhibit higher ductility. EBFs with WF links reach peak reaction force at the 29th cycle, with performance declining by the 32nd cycle. In contrast, HSD link EBFs peak at the 31st cycle, maintaining performance longer. The average ductility performance of HSD link EBFs is 19.9% higher than that of WF link EBFs.

REFERENCES

1. Montouri, R., Nastri, E., and Pilusi, V., Theory of Plastic Mechanism Control for Eccentrically Braced Frames with Inverted Y-Scheme, *Journal of Constructional Steel Research*, *92*(January), 2014, pp. 122–135.
2. Bruneau, M, Uang, C.M., and Sabelli, R., *Ductile Design of Steel Structures*, 2011, McGraw Hill, New York.
3. Suswanto, B. and Wahyuni, E., Numerical Behavior Study of Short Link, Intermediate Link, and Long Link in Eccentrically Braced Frames Steel Structure, *International Journal of Applied Engineering Research*, *12*(21), 2017, pp. 11460–11471.
4. Mansour, N., Christopolous, C., and Tremblay, R., Experimental Validation of Replaceable Shear Links for Eccentrically Braced Steel Frames, *Journal of Structural Engineering*, *137*(10), 2011, pp. 1141–1152.
5. Musmar, M.A., Effect of Link on Eccentrically Braced Frames, *Journal of Engineering Sciences*, *40*(1), 2012, pp. 35–43.
6. Tan, K., *Replaceable Cast Steel Links for Eccentrically Braced Frames*, 2014, University of Toronto.
7. Suswanto, B., Rafael, J., and Sutrisno, W., *Eccentrically Braced Frames Structural Systems* (In Indonesia), 2018, ITS Press, Surabaya.
8. Bosco, M.R.P. and Rossi, P.P., Seismic Behaviour of Eccentrically Braced Frames, *Engineering Structure, 31*(3), 2009, pp. 664–674.
9. Mansour, N., Shen, Y., Christopoulos, C., and Tremblay, R., Experimental Evaluation of Nonlinear Replaceable Links in Eccentrically Braced Frames and Moment Resisting Frames, in *The 14th World Conference on Earthquake Engineering*, 2008, Beijing, China.
10. Wang, F., Su, M., Hong, M., Guo, Y., and Li, S., Cyclic Behaviour of Y-Shaped Eccentrically Braced Frames Fabricated with High-Strength Steel Composite, *Journal of Constructional Steel Research*, *120*(April), 2016, pp. 176–187.
11. Shayanfar, M., Rezaeian, A.R., and Zanganeh, A., Seismic Performance of Eccentrically Braced Frames with Vertical Link using PBPD Method, *The Structural Design of Tall and Special Buildings*, 2012.
12. Bouwkamp J., Vetr, M.G., and Ghamari, A., An Analytical Model for Inelastic Cyclic Response of Eccentrically Braced Frame with Vertical Shear Link, *Case Studies in Structural Engineering*, *6*, 2016, pp. 31–44.
13. Daneshmand, A. and Hashemi, B.H., Performance of Intermediate and Long Links in Eccentrically Braced Frames, *Journal of Constructional Steel Research, 70*(March), 2012, pp. 167–176.
14. Vetr, M.G., Ghamari, A., and Bouwkamp, J., Investigating the Nonlinear Behavior of Eccentrically Braced Frame with Vertical Shear Links (V-EBF), *Journal of Building Engineering*, *10*(March), 2017, pp. 47–59.
15. TahamouliRodsari, M., Eslamimanesh, M.B, Entezari, A.R., Noori, O., and Torkaman, M., Experimental Assesment of Retrofitting RC Moment Resisting Frames with ADAS and T-ADAS Yielding Dampers, *Structures*, *14*, 2018, pp. 75–87.
16. Aghlara, R., Tahir, M., and Adnan, A., Comparative Study of Eight Metallic Yielding Dampers, *Jurnal Teknologi*, *77*(16), 2015, pp. 119–125.
17. Kamura, H., Nanba, K, Oki, K., and Funaba, T., Seismic Response Control for High-Rise Buildings Using Energy-Dissipation Devices, *JFE Techical Report*, 2009.
18. Benavent-Climent, A., Brace-type Seismic Damper Based on Yielding the Walls of Hollow Structural Sections, *Engineering Structures*, *32*(4), 2018, pp. 532–539.
19. Teruna, R., Majid, T., and Budiono, B., Experimental Study of hysteresis Steel Damper for Energy Dissipation Capacity, *Advances in Civil Engineering*, 2015.
20. Moestopo, M., Kusumastuti, D., Lim, E., Akbar, U., and Ramadhita, M.S., Experimental Study on the Seismic Behavior of Replaceable Shear Links Connected to Coupling Beam, *International Journal on Advanced Science Engineering Information Technology*, *8*, 2018, pp. 532–539.
21. AISC, Seismic Provisions for Structural Steel Buildings, ANSI/AISC 341-10. In: *Structural Analysis and Design of Tall Buildings*, CRC Press, 2011, pp 355–410.
22. Wang, W., Cai, H., Bai, C., Bao, H., Gao, B., Yuan, Z., and Wang, K., Seismic performance of Partially Encased Concrete Composite Columns with Corrugated Web, *Journal of Building Engineering*, *77*, 2023. https://doi.org/10.1016/j.jobe.2023.107481
23. Suswanto, B., Ghifari, F., Tajunnisa, Y., and Iranata, D., Retrofitting Bolted Flange Plate (BFP) Connections using Haunches and Extended End-Plates, *Civil Engineering Journal*, *10*(8), 2024, pp. 2450–2470.